CORROSION PROTECTION DESIGN OF SEAWATER PUMP BY BOUNDARY ELEMENT ANALYSIS SYSTEM

by

Matsuho Miyasaka

Deputy General Manager

Ebara Research Company, Ltd.

Fujisawa, Japan

Hirokazu Takayama

Manager

Ebara Corporation

Tokyo, Japan

Kenji Amaya

Associate Professor

and

Shigeru Aoki

Professor

Tokyo Institute of Technology

Tokyo, Japan

Matsuho Miyasaka is a Deputy General Manager in the Center for Technology Development, Ebara Research Company, Ltd., in Fujisawa, Japan. He has been engaged in preventing marine corrosion and developing corrosion resistant materials, and has developed a boundary element analysis system for corrosion protection design with Professor Aoki's group of the Tokyo Institute of Technology, Japan.

Dr. Miyasaka graduated from the Metallurgical Engineering Department of Tohoku University (1972), and has a Doctor degree from the Tokyo Institute of Technology (1994). He is a member of NACE, AWS, and JSCE.

Hirokazu Takayama is a General Manager in the Production System & Engineering Division for Ebara Corporation, in Tokyo, Japan. He has been engaged in the practical application of numerical corrosion-analysis techniques and the development of the analysis system.

Mr. Takayama has B.S. (1973) and M.S. (1975) degrees from the Metallurgical Engineering Department of Kansai University, in Osaka, Japan.

Kenji Amaya is an Associate Professor in the Graduate School of the Tokyo Institute of Technology, in Tokyo, Japan. He has been interested in corrosion analysis and inverse analysis.

Dr. Amaya has a Doctor degree from the Tokyo Institute of Technology (1993).

ABSTRACT

A computer aided corrosion-analysis-system to which boundary element method (BEM) is applied has been developed, and is utilized for diagnosing galvanic corrosion and designing cathodic protection of seawater and brine pumps. Using the BE analysis technique, potential and current density distributions on the object can be calculated under three conditions:

- 3-D geometry of the object,
- Polarization curves (relationship between current density and potential, which is measured in the laboratory) of pump materials and sacrificial anodes, and
- Conductivity of the solution.

Hence, it is possible to estimate the protective effectiveness with the potential distribution, and the life of sacrificial anodes for cathodic protection and the corrosion rate of galvanic corrosion

can be calculated with the current densities. The BE analysis system consists of:

- Element segmentation software,
- Input file preparation software,
- Boundary element analysis software,
- Input/output data graphic software, and
- Polarization curve database.

The quantitative corrosion predictions obtained with this analytic system make it possible to rationalize corrosion protection design and maintenance, improve the operational reliability of machinery, and reduce cost.

INTRODUCTION

Seawater is widely used as cooling water at power plants, steel manufacturing, and chemical plants, etc., and as material and cooling water at seawater desalinization plants and salt manufacturing plants. Seawater pumps are an important constituent of these plants. Seawater contains a large amount of inorganic salts, primarily chloride, and has a high conductivity. Because of these two reasons, seawater is highly corrosive; thus, it is important to find ways to protect seawater pumps against corrosion.

Since seawater is highly conductive, seawater pumps are easily damaged by galvanic corrosion. At the same time, cathodic protection can be effectively applied in seawater. The prediction of:

- Rates of galvanic corrosion,
- The extent to which corrosion can be prevented by cathodic protection, and
- The life of sacrificial anodes

is of extreme importance from the point of view of maintenance of seawater and brine pumps.

Such predictions have been based traditionally on past experience, which required large safety factors. Following an increase in computer processing power, numerical methods such as boundary element method (BEM) (Danson and Warne, 1983; Aoki, et al., 1985; Zamani, et al., 1986; Aoki, et al., 1988; Miyasaka, et al., 1995a, 1995b, 1995c; Aoki, et al., 1999; Gartland, et al., 1999; Adey and Hang, 1999) and finite element method (FEM) (Strommen, 1979; Kasper, 1983) have been applied to solve corrosion problems. Because the knowledge of physical quantities (potential and current density) on the surface of corroding materials is of prime importance in corrosion and corrosion prevention, the authors have developed a BEM that does not require discretization of internal elements, and have shown the usefulness of the BEM by analyzing galvanic corrosion, differential-aeration-cell corrosion, and cathodic protection. Based on this BE analysis technique, the authors have developed a corrosion-analysis-system.

In considering corrosion problems of fluid machines such as pumps, analyses should take into account the polarization characteristics of materials under high flow-velocity conditions, but so far no analyses of machines handling high flow-velocity solutions have been observed. The authors have first applied the BEM to the analyses of corrosion problems of a pump, which is a fluid machine with complex 3-D fields.

This report describes mechanisms of galvanic corrosion and cathodic protection, a numerical analysis technique of corrosion problems using BEM, an outline of the BE analysis system, and analysis examples of cathodic protection design of a seawater pump.

MECHANISMS OF CORROSION AND PROTECTION

Metal corrosion in an aqueous solution advances as a result of an electrochemical reaction that pairs together an anodic reaction and cathodic reaction. For example, the corrosion reaction of iron in seawater or other neutral solutions containing dissolved oxygen can be represented by Equations (1) and (2). Equation (1) shows the dissolution reaction (corrosion reaction) of Fe, and Equation (2) shows the reduction reaction of the dissolved oxygen.

$$Fe \rightarrow Fe^{2+} + 2e \quad \text{(anodic reaction)} \tag{1}$$

$$\tfrac{1}{2} O_2 + H_2O + 2e \rightarrow 2OH \quad \text{(cathodic reaction)} \tag{2}$$

On a metal surface, the place where anodic reaction occurs is called the anode, and the place where cathodic reaction occurs is called the cathode. When iron corrodes in seawater, the area of each anode and cathode is usually very small, the locations of them are intermixed, and their positions are not fixed. As a result, corrosion, while accompanied by some surface unevenness, advances fairly uniformly over an entire area. If, however, the materials, surface conditions, and environmental conditions are not the same or are not uniform, the anodes and cathodes will become unevenly distributed and corrosion will concentrate in certain areas (anodes). The former corrosion form is classified as microcell corrosion, and the latter is classified as macrocell corrosion. These two types of corrosion are illustrated in Figure 1. The type that most often causes large damage to seawater pumps is macrocell corrosion, including galvanic corrosion and differential-aeration-cell corrosion, and other localized corrosions.

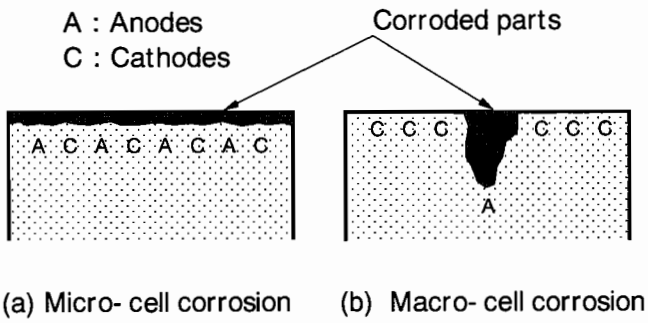

Figure 1. Illustration of Microcell and Macrocell Corrosion.

Where there are two different kinds of materials in aqueous solution, corrosion occurs exclusively on the specified anodic material. This mode of corrosion is defined as galvanic corrosion. On the other hand, cathodic material is protected by the sacrificial anodic material. This corrosion protection behavior is utilized as cathodic protection.

A specific example is given to help understand galvanic corrosion and cathodic protection. Consider a rectangular container such as the one shown in Figure 2(a) ($0.1 \times 0.1 \times 0.2$ m^3). Assume that steel and stainless steel (SS) are set opposite each other on both ends, electrical continuity is established, and the container is filled with a NaCl solution (electric conductivity: 0.0357 S/m). In this galvanic system, the steel acts as anode, and the SS acts as cathode. Figure 2(b) shows the polarization curves of both materials measured under an identical solution environment (25°C, flow-velocity of zero). The current axis is shown in this figure as the total current on the electrode surface (0.01 m^2).

Solution resistance, R_s, between the electrodes is calculated as follows:

$$R_s = \frac{L}{\kappa \times A} \tag{3}$$

Here, R_s is the resistance of the solution (Ω), κ is the electric conductivity (S/m), L is the length (m), and A is the area (m^2). Thus, $R_s = 0.2 / (0.0357 \times 0.1 \times 0.1) = 560$ (Ω). If we use these values in the calculation, we find that the galvanic current (I_G) flowing from the SS electrode to the steel electrode through the lead

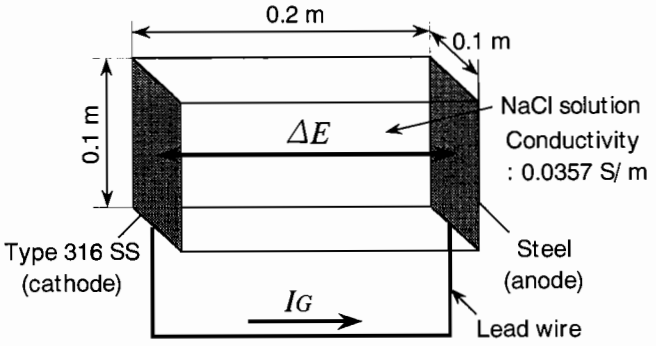

(a) Galvanic system of type 316 SS and steel

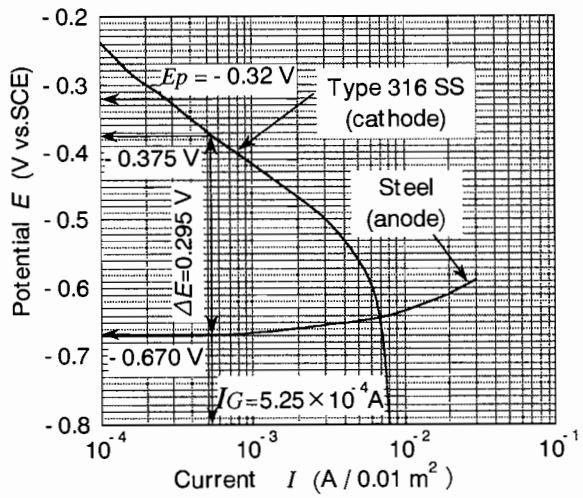

(b) Polarization curves

Figure 2. Prediction of Potential and Current in a Simple Galvanic System.

wire (Figure 2(a)) and the potential difference (ΔE) between the electrodes through the solution, become balanced under Equation (4) at approximately 5.25×10^{-4} A and 0.295 V, respectively.

$$\Delta E = I_G \times R_S \quad (4)$$

Therefore the potentials on the surfaces of the SS and the steel become approximately -0.375 and -0.670 V versus saturated calomel electrode (SCE) (hereinafter, SCE is used as the reference electrode), respectively. The galvanic current I_G of 5.25×10^{-4} A causes the steel to corrode via the promotion of galvanic corrosion, while conversely protecting the SS from corrosion. The potential of -0.375 V on the SS is less noble than the corrosion protection potential E_P of the type 316 SS in seawater (-0.32 V) (Tsujikawa, et al., 1981), and the E_P in the lower chloride ion containing water should be nobler. Thus, the type 316 SS is protected against corrosion such as pitting and crevice corrosion. If we calculate the extra steel corrosion (galvanic corrosion) from this 5.25×10^{-4} A of current I_G (current density: 5.25×10^{-2} A/m^2), we get 0.06 mm/y. In this case, however, there is very little galvanic corrosion because the area ratio of cathode (SS) to anode (steel) is the small value of one. Galvanic corrosion rate increases with the increase in the area ratio of cathode to anode. The rate of total steel corrosion is the value obtained by adding the amount of self-corrosion to this value.

Figure 3 shows a severe galvanic corrosion example of a seawater pump. A small-area cast-iron part (bearing casing) made contact with a large-area SS part and corroded as much as 25 mm during a 22-month period. The example shows that galvanic corrosion damage can be extremely large when the area ratio, the area of the cathode (SS) compared to that of the anode (cast-iron), is large. In this case, the galvanic corrosion problem was solved by the exchange of the bearing housing from cast-iron to SS. Insulation between the different materials is also effective in protecting the pump parts from galvanic corrosion. It is desirable to be able to accurately predict galvanic corrosion ahead of time and to take appropriate measures.

Figure 3. Galvanic Corrosion Example of Seawater Pump.

Figure 4 shows an example of cathodic protection applied to a vertical seawater pump. The cathodic protection design is desired to be rationally conducted based on the kinds and locations of anode materials, the shape of the pump, materials combination, and the solution conditions (conductivity, flow-velocity, etc.).

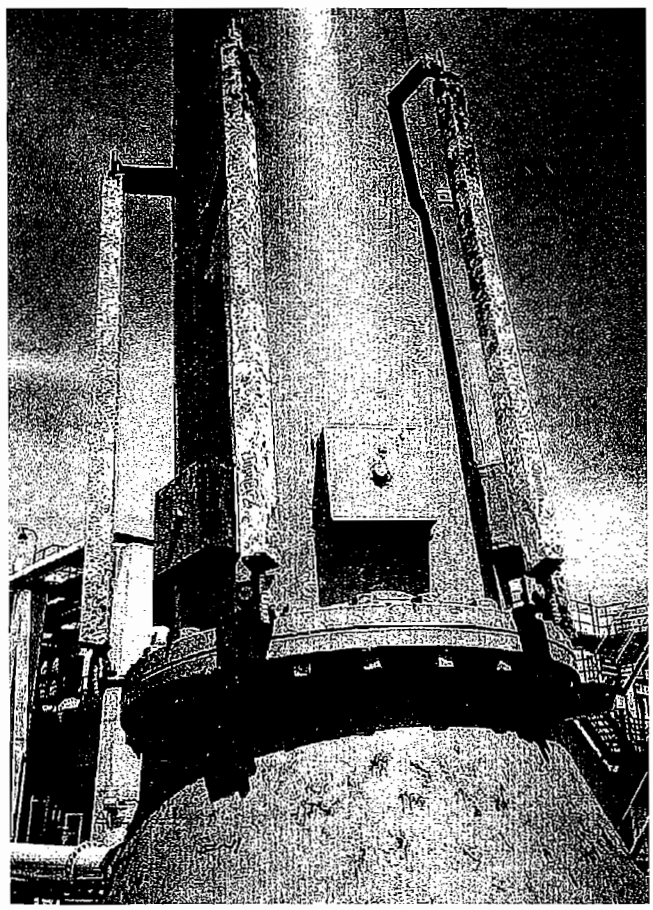

Figure 4. Example of Cathodic Protection Applied to a Vertical Seawater Pump. (Four prismatic Zn anodes are attached outside the column pipe.)

BOUNDARY ELEMENT ANALYSIS

Necessity of Numerical Analysis

Basically, corrosion and corrosion protection can be evaluated using the polarization curves with the process shown in Figure 2(b). In reality, however, such a simple system as that shown in Figure 2(a) is hardly ever seen, and macrocell behavior is more complex and difficult to predict.

Because the 3-D shape of the region occupied by the electrolyte greatly affects macrocell behavior, it is difficult to accurately estimate the resistance through the solution in complex structures. Experiment-based methods are also limited in their capacity to accurately predict corrosion and corrosion protection involving actual equipment and structures.

Hence, in a large number of cases, past experiences have been relied on for the prediction of macrocell corrosion and cathodic protection of actual structures. In recent years, however, analytical research has flourished in order to provide more accurate quantitative predictions. As an analytical procedure, the authors chose BEM, which does not require discretization of internal elements.

Basic Equation and Boundary Conditions

As explained in the preceding section, both galvanic corrosion and cathodic protection can be thought of in terms of a cell formed by an anode, cathode, and electrolyte. Assume that an electrolyte is surrounded by boundaries Γ_1, Γ_2, Γ_a, and Γ_c (Figure 5), where Γ_1 is the boundary at which the value of potential, ϕ, is ϕ_0 (boundary of fixed potential), Γ_2 is the boundary at which the value of current density, i, is i_0 (boundary of fixed current density), and Γ_a and Γ_c are the surfaces of the anode and cathode, respectively. The potential field throughout the region filled with the electrolyte may be mathematically modeled by Laplace's equation (Equation (5)) under boundary conditions Equation (6) through Equation (9):

$$\nabla^2 \phi = 0 \tag{5}$$

$$\phi = \phi_0 \quad \text{on } \Gamma_1 \tag{6}$$

$$i\left(\equiv \kappa \frac{\partial \phi}{\partial n}\right) = i_0 \quad \text{on } \Gamma_2 \tag{7}$$

$$\phi = -f_a(i) \quad \text{on } \Gamma_a \tag{8}$$

$$\phi = -f_c(i) \quad \text{on } \Gamma_c \tag{9}$$

where κ is the conductivity of the electrolyte, and $\partial/\partial n$ is the outward normal derivative. $f_a(i)$ and $f_c(i)$ are nonlinear functions that respectively indicate the experimentally determined polarization curves for the anode (Γ_a) and cathode (Γ_c).

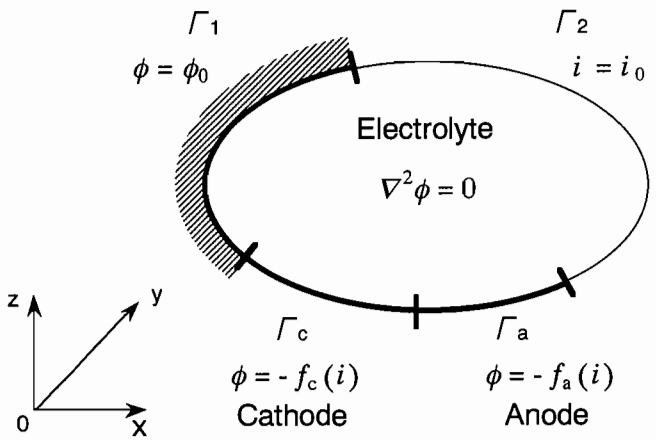

Figure 5. Basic Equation and Boundary Conditions for Boundary Element Analysis.

Here, the relationship between the electric potential, ϕ, used in the analysis and the electrode potential, E, that we actually measure can be expressed as follows: $\phi = -E$. If Equation (5) is solved based on the boundary condition Equation (6) through Equation (9), the potential and current density distribution near the surface can be found.

For simplicity, the foregoing explanation discusses cases involving two types of metal, but three or more types of metal can be handled in the same manner. Equation (5), the Laplace equation, is a partial differential equation that is regularly utilized for problems involving steady heat conduction and problems involving the irrotational flow of incompressible fluids. A feature of corrosion protection problems, however, is that the boundary conditions for the anode and cathode are nonlinear.

Boundary Element Formulation

Following the normal formulation of the BEM leads from Equation (5) to the following boundary integral Equation (10). Let P and Q be two points inside or on the surface of Ω, and let ϕ^* be the known fundamental solution with singularity at Q. Taking $\phi^* \times \nabla^2\phi$ to be integrated over Ω, with Q located on Γ, and applying two successive integrations by parts yield:

$$\kappa c\phi = \int_\Gamma (i\phi^* - \phi i^*)\, d\Gamma \tag{10}$$

where $i^* = \kappa \partial\phi^*/\partial n$, and c is the known constant resulting from the Cauchy principal value of the surface integral. Surface Γ is discretized into boundary elements, and values of ϕ and i are approximated in terms of interpolation functions and nodal values.

By adopting the standard procedure of BEM, the following simultaneous algebraic equations are obtained:

$$[A]\begin{bmatrix} x_j \\ i_j \end{bmatrix} = [B]\begin{bmatrix} b_j \\ f_i(i_j) \end{bmatrix} \tag{11}$$

where x_j values ($j = 1, 2, \ldots, p$) are the unknown values of ϕ or i on $\Gamma_1 + \Gamma_2$, and b_j ($j = 1, 2, \ldots, p$) are the given values on $\Gamma_1 + \Gamma_2$. The functions $f_j(i_j)$ ($j = 1, 2, \ldots, s$) are the nonlinear functions representing the polarization curves. $[A]$ and $[B]$ are matrices geometrically determined on boundary Γ. The numbers of elements on $\Gamma_1 + \Gamma_2$ and $\Gamma_a + \Gamma_c$ are respectively indicated by p and s. The above nonlinear equations are solved by using the Newton-Raphson iterative method.

Development of Analysis Programs

The authors have engaged in the development of BE analysis techniques for corrosion and corrosion protection since the early 1980s, and have developed analysis programs that handle 2-D, 3-D, and axisymmetric closed and open regions. Through analyses and verification experiments using models and actual pumps, the programs have been shown to be effective in predicting galvanic corrosion, differential-aeration-cell corrosion (differential-flow-velocity-cell corrosion), and cathodic protection.

VERIFICATION OF ANALYSIS PROGRAM

The applicability of the BE analysis program (Miyasaka, et al., 1995a, 1995c) to fluid machines handling seawater with complex 3-D fields is examined in this section. Experiments and analyses are carried out on cathodic protection system in a seawater pump. It is shown that a highly accurate analysis can be performed by considering flow-velocity and time dependencies of polarization curves.

Cathodic Protection Experiments Performed on Vertical Seawater Pump

The pump used in the experiments was a vertical pump with 200 mm nozzle diameter and 6.5 m overall length, shown in Figure 6. Figure 7 is a photograph of the pump. The materials of the components

were as follows: suction bell, casing liner, guide casing, column pipe, shaft enclosing tube, and other stationary parts were made of gray cast-iron. Impeller, shaft, and other rotating parts were made of type 316 SS. Zinc (Zn) sacrificial anodes were attached to two locations inside the pump (one inside the suction bell and the other inside the column pipe). The pump was run continuously pumping 2.5 m^3/min of seawater for 480 hr. This meant that the average flow-velocity inside the column pipe was 1.5 m/s. The pump rotating speed was 1440 rpm, and the circumferential speed of the impeller was approximately 15 m/s. The stationary parts of the pump are, in fact, normally insulated from the rotating parts while the pump is running (without the need for special insulators), but insulators were provided to ensure perfect insulation conditions in the experiment.

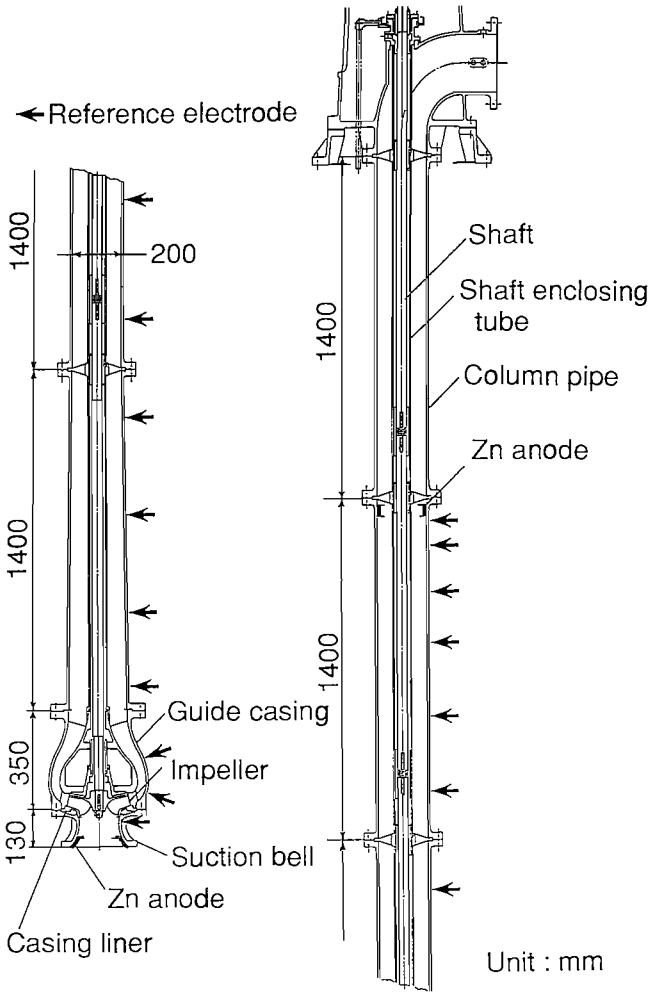

Figure 6. Tested Vertical Seawater Pump and Location of Zn Anodes.

The exposed areas of the Zn anodes inside the suction bell and the column pipe were 265 cm^2 and 199 cm^2, respectively. The Zn anodes were not in direct contact with the pump body; but the Zn anodes and the pump body were electrically connected with a zero-shunt ammeter and an automatic changeover switch. Thus, anodic currents on the Zn anode surfaces were continuously measured. Reference electrodes for the potential measurement were fitted in the positions indicated by the arrows in Figure 6.

Only flowpath surfaces were not coated, with outer surfaces being coated with coal tar-epoxy resin. Average coating thickness was 345 μm. Average seawater temperature in the test duration was 25°C. The conductivity, κ, was 4.5 S/m at 25°C (which was then used in the computation). Experimental results are shown later in the paragraph in which comparisons are made with analysis results.

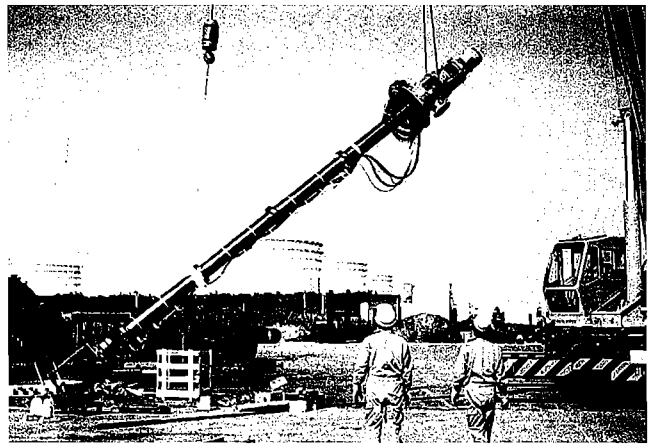

Figure 7. Actual Seawater Pump Used to Measure the Potential Distribution Inside the Pump and Current Densities of the Zn Anodes.

Polarization Measurements

The polarization characteristics of cast-iron and Zn anode in seawater were investigated, using a parallel-flow type corrosion test cell with rectangular flowpaths and a glass beaker (when flow-velocity was zero). Regarding cast-iron: first the potentiodynamic cathodic and anodic polarization curves were measured in a flow-velocity range of 0 through 15 m/s. The purpose of these measurements was to ascertain the flow-velocity dependency of polarization curves, in a relative manner. The measurements were started after 10 min of exposure. The scanning rate was 1.8 V/h. Following this, potentiostatic (−0.8 V and −1.0 V) polarization measurements were conducted at the flow-velocities of 0, 1.5, and 15 m/s, for a maximum of 336 hr, in order to determine the time dependency of cathodic polarization characteristics. In addition, time dependency of natural potentials was examined for a maximum of 336 hr. Regarding Zn anodes: it was thought that the time dependency of anodic polarization curves would be comparatively slight. Therefore, only potentiodynamic anodic polarization measurements were conducted, in a 0 through 2 m/s range. The measurements were started after 18 hr of exposure.

Figure 8 shows the flow-velocity dependency of the potentiodynamic cathodic polarization curves. As flow-velocity increases, natural potentials shift to a more noble direction, and simultaneously the current density shows a marked increase. The anodic polarization curves for both cast-iron and Zn shifted to the more noble direction almost in parallel in response to the rise in flow-velocity. The anodic polarization curves of Zn had only a small dependency on flow-velocity.

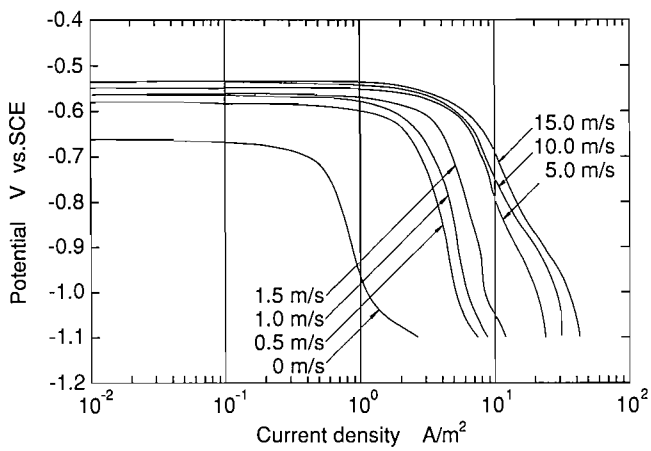

Figure 8. Potentiodynamic Polarization Curves of Cast-Iron in Seawater at 25 ℃, Changing with the Change in Flow-Velocity.

Figure 9 shows the change in current density for cast-iron under potentiostatic polarization. In seawater, the current density on the cathode gradually drops as time passes. This time dependency of cathodic current density occurs because, in the cathodic reaction ($^1/_2 \cdot O_2 + H_2O + 2 \rightarrow 2OH^-$), the alkalinity of the surface of the cathode increases; then $CaCO_3$ and $Mg(OH)_2$ are deposited as scale, which restricts the diffusion of dissolved oxygen. Figure 10 shows scanning electron microscope (SEM) images of the surface of cast-iron specimens that have been polarized at −0.8V (a) at flow-velocity of 1.5 m/s for 336 hr, and (b) at a flow-velocity of zero for 168 hr. Scale formed on the surface in both cases.

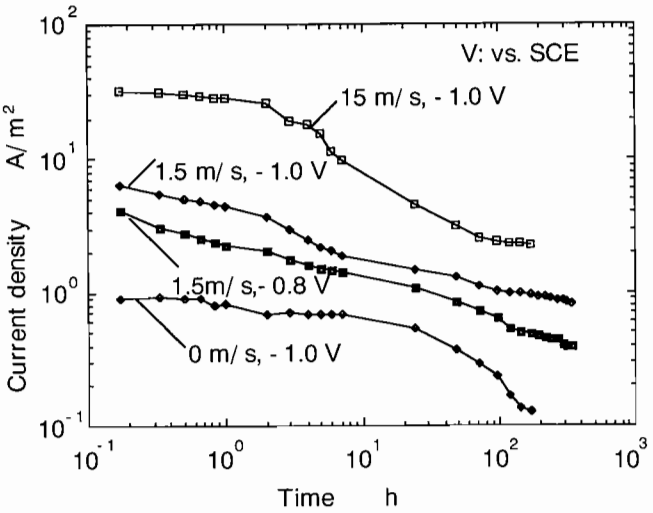

Figure 9. Potentiostatic Polarization Behavior of Cast-Iron in Seawater at 25 ℃.

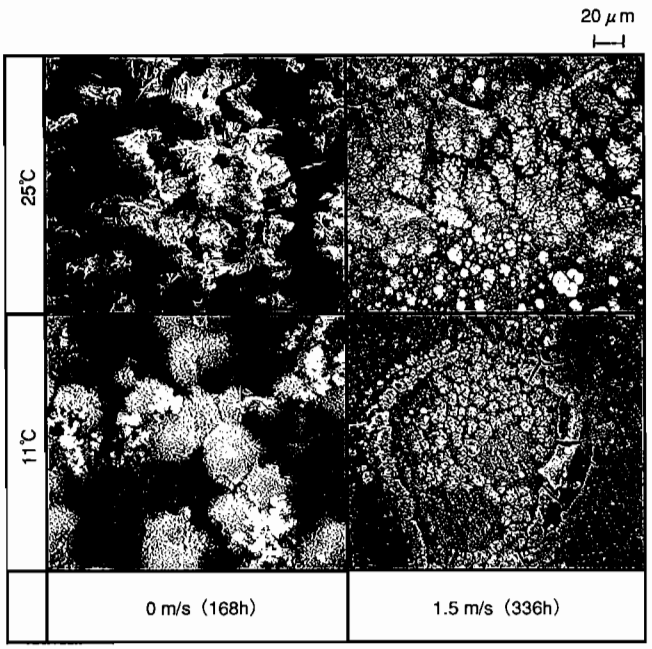

Figure 10. SEM Images of the Surface of Cast-Iron Specimens That Have Been Cathodically Polarized.

Boundary Element Discretization

BE analyses were performed on the cathodic protection experiment, and the analysis results were compared with the experimental data. Figure 11 shows the boundary element discretization of (a) inside the guide casing and its vicinity and (b) inside the column pipe. The shapes of the parts in the vicinity of the guide casing are particularly complex, and need to be modeled appropriately in order to carry out an effective analysis. The inside of the guide casing is divided into six flowpaths by six guide vanes. Current does not pass through these guide vanes, moreover, the six zones formed by the guide vanes are mutually equivalent. Therefore, the authors selected just one of the six flowpaths inside the guide casing, and performed element discretization on it. The same reasoning was used in dealing with the impeller. They performed element discretization of only a 60-degree section of the upper part of the guide casing and the lower part of the impeller. Also, on the outside of the guide casing, galvanic current flows, but the fluid flow-velocity was almost zero, and the outside of the casing was coated. It was therefore judged that current density on the outside of the casing would be extremely low, thus, only the inside of the guide casing was analyzed. Because inside the column pipe can be treated as being axially symmetric, the authors did not carry out the analyses for all 360-degrees of the pipe cross section, but limited analysis to a 60-degree section only (axisymmetric analysis can also be performed now).

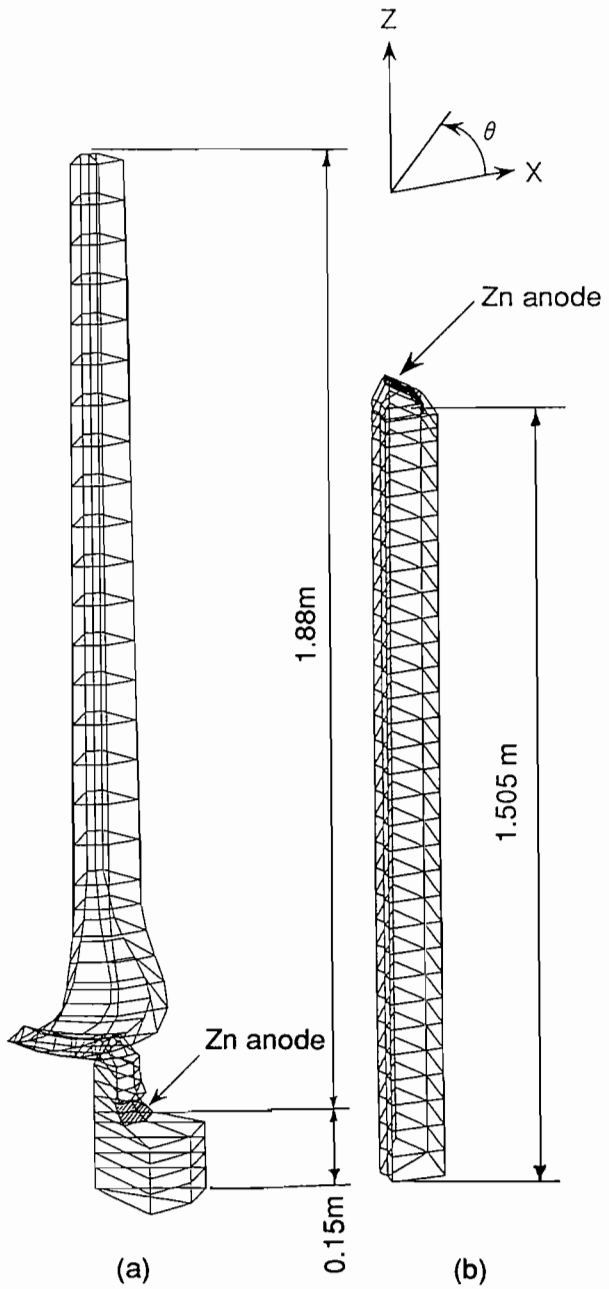

Figure 11. Boundary Element Discretization.

Boundary Conditions

Each element for the pump body had to be assigned the polarization curves appropriate for the flow-velocity at that element as boundary conditions. Taking as reference values:

- The current densities (at −0.8 V and −1.0 V) obtained in the potentiostatic current measurements, and
- The natural potentials measured after 18 hr (it was ascertained from the measurement of change in natural potential that the potentials have fully stabilized after 18 hr),

the authors constructed approximate polarization curves of cast-iron. In the case of flow-velocities at which potentiostatic current measurements had not been performed, they extrapolated from the dependency on flow-velocity indicated by the potentiodynamic polarization curves, in order to construct approximate polarization curves at these flow-velocities. For the approximate polarization curve of the Zn anode, the potentiodynamic polarization curve at the flow-velocity of 2.0 m/s was applied.

The pump interior was divided into four flow-velocity zones (1.0, 1.5, 2.0, and the highest flow-velocity being 15 m/s on the surface of the casing liner), and each zone was assigned the approximate polarization curve as its boundary condition. Figure 12 shows an example of approximate polarization curves used in the analysis of the guide casing (at 72 hr). The impeller and other rotating parts were insulated from the cast-iron parts and Zn anodes. Therefore, these elements were assigned "insulated" as their boundary condition. Boundary condition $i_0 = 0$ was assigned to the insulated elements.

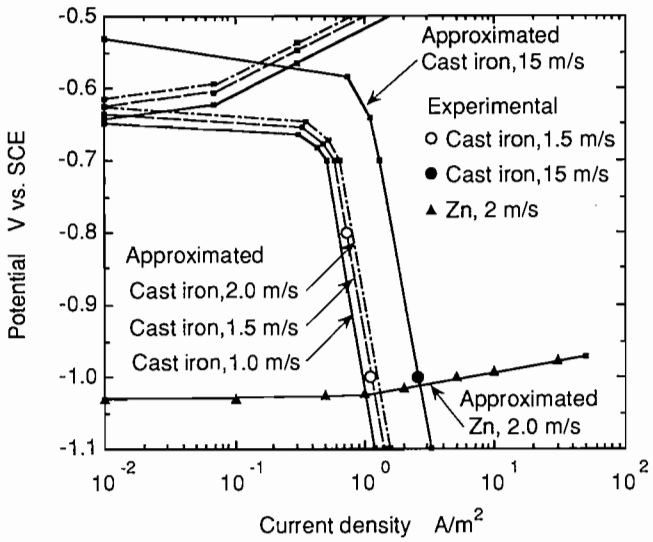

Figure 12. Approximated Polarization Curves for Analysis on Guide Casing and Its Vicinity.

Comparison Between Calculated and Experimental Results

Figure 13 shows the calculated results and experimental data of potential distribution in the vicinity of the guide casing. Good agreement is obtained between the predicted and experimental results. Figure 14 shows the same results for inside the column pipe. The calculated results predict with high accuracy the manner in which the corrosion-inhibited area spreads with time. One reason for the narrow corrosion-inhibited area in the guide casing as compared to the inside of the column pipe is the existence of the casing liner. In other words, the reason is that the particularly high flow-velocity (15 m/s) on the surface of this part produces a high cathodic current density, resulting in a steep potential.

Figure 15 shows a comparison of the calculated and experimental results for the anodic current density on the surfaces of the Zn anodes. Consumption rates of the Zn anodes calculated from the current densities are also shown in Figure 15. It is seen that highly-accurate analysis results were obtained.

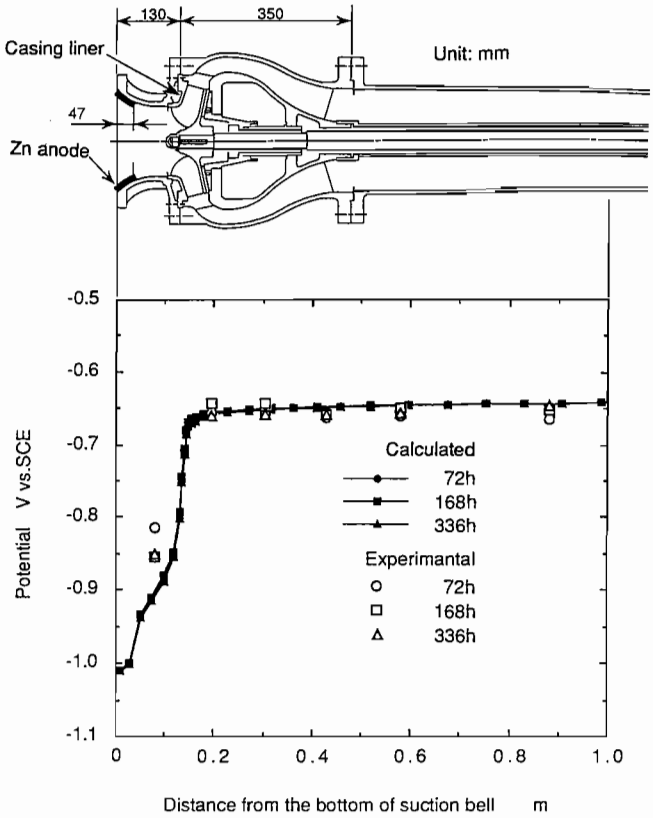

Figure 13. Comparison Between Calculated and Experimental Potential Distribution Inside Guide Casing and Its Vicinity.

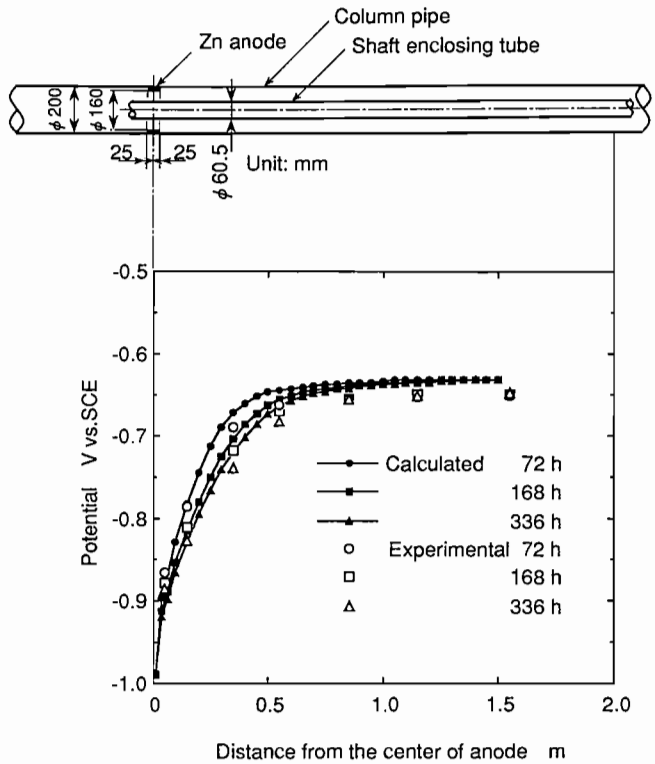

Figure 14. Comparison Between Calculated and Experimental Potential Distribution Inside Column Pipe.

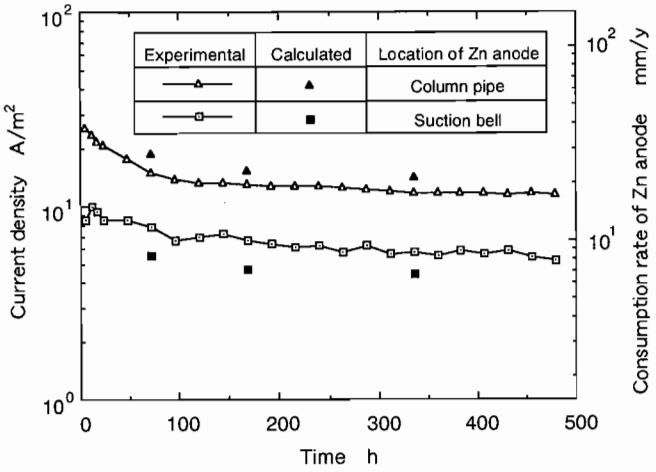

Figure 15. Comparison Between Calculated and Experimental Current Densities On the Surface of Zn Anodes.

BOUNDARY ELEMENT ANALYSIS SYSTEM

In order to conduct analyses more efficiently, the authors developed an analysis system. Currently, this system is being utilized to diagnose corrosion and corrosion protection design of equipment (primarily seawater pumps) used in corrosive environments. The system structure and analysis examples will be introduced next.

System Structure

Figure 16 shows the sequence of the BE analysis system. The system consists of:

1. Element segmentation software,
2. Input file preparation software,
3. Boundary element analysis software,
4. Input/output data graphic software, and
5. Polarization-curve database.

Element discretization can be done automatically using 3-D computer-aided-design (CAD) software. Input files are constructed by setting up polarization curves for each element and specifying the conductivity of the solution; however, these operations are performed interactively using a computer terminal. If you enter the material, flow-velocity, and time, a polarization curve database will be processed and the specified number of polarization curves (corresponding to the material and flow-velocity) will be created in the input files.

The polarization-curve database incorporated into this system was created based on potentiodynamic polarization curves (example in Figure 8) obtained through measurements taken in seawater flowing at 0 through 15 m/s for various practical materials, such as cast-iron, austenitic cast-iron, stainless steel, and copper alloy, as well as aluminum and zinc sacrificial anodes. Interpolating measured flow-velocity data makes it possible to create arbitrary flow-velocity data. In seawater, the current density on the cathode gradually drops as time passes. To reflect this phenomenon, polarization curves are automatically created corresponding to the specified time and are based on empirical formulas showing the time dependency of the cathodic current density found by the potentiostatic cathodic polarization measurement (example in Figure 10).

This system can be used to analyze closed and open regions that are 2-D, 3-D, and axisymmetric. The analysis conditions can be displayed as input data, such as element-discretization wire frame diagrams, color-coded diagrams by material or polarization characteristic, and polarization curves used for analysis. The

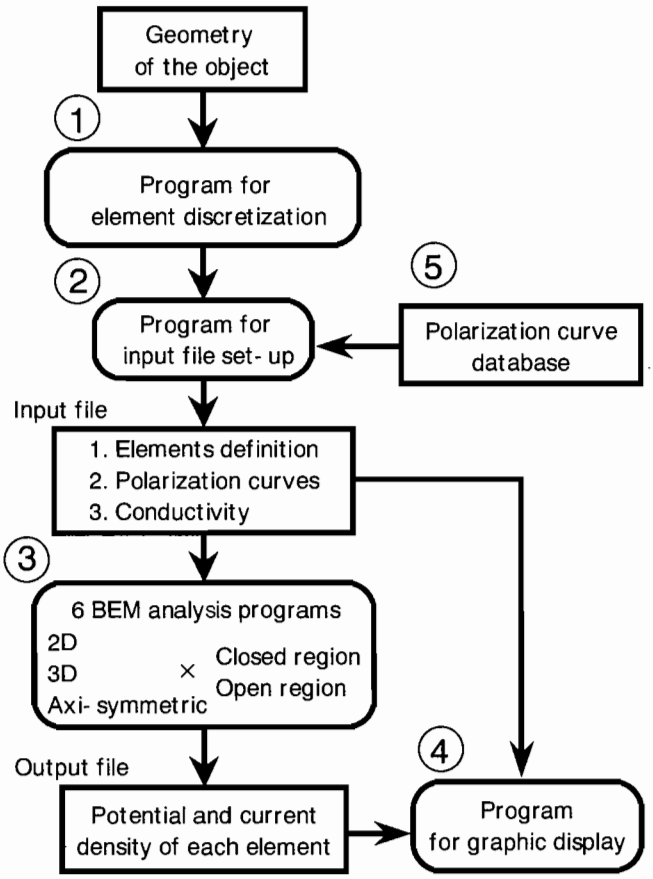

Figure 16. Sequence of the Boundary Element Analysis System.

analysis results can also be displayed in color as output data, such as potential distributions; current density distributions; diagrams that distinguish between complete corrosion protection regions (less noble than the protective potential, E_p), corrosion control regions (between natural potential and the protection potential), and corrosion promotion regions (nobler than natural potential); and corrosion rate (including anode consumption rate) display diagrams.

Analysis Examples

Here will briefly be introduced the flow of the analysis being applied to cathodic protection design for a vertical seawater pump. As shown in Figure 17, the analysis object was a 700 mm bore-type 316 SS vertical seawater pump (uncoated). The effect of corrosion protection and life of the sacrificial anodes were predicted using zinc sacrificial anodes for cathodic protection. Three round zinc anodes were attached inside the pump: one each at two locations on the interior surface of the column pipe, and one on the inner surface of the suction bell. Four prismatic zinc anodes were attached outside the pump (same example in Figure 4).

The pump interior surface was analyzed as a 3-D closed region. Element discretization of the pump interior was done in the same manner described in Figure 11. To simplify the analysis of the outer surface of the pump, the four prismatic Zn anodes were approximated by a circular ring with the same area. In doing so, the outer pump surface was treated as an axisymmetric open region. A combined analysis between the exterior and interior regions was conducted (Miyasaka, et al., 1998). The pump interior has a complex flow-velocity distribution, but in this study, it was divided into four flow-velocity regions (1.3, 1.8, 3.7, and 6.7 m/s). Type 316 SS and Zn polarization curves corresponding to these flow-velocities were assigned to each element as a boundary condition. A flow-velocity of zero was applied to the polarization curves for the outer surface of the pump, because there was practically no

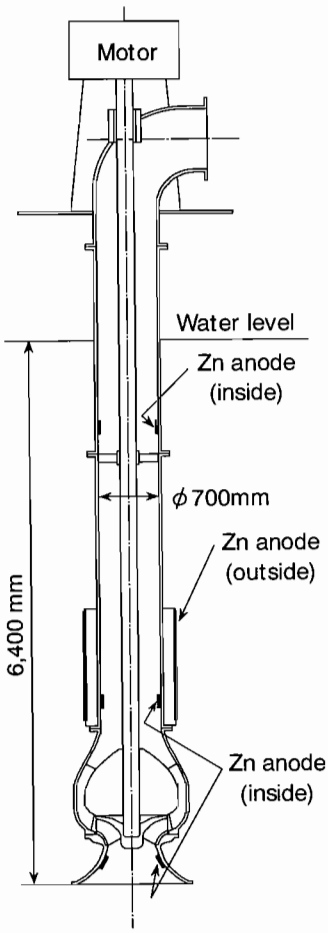

Figure 17. Analysis Object: Type 316 Stainless Steel Vertical Seawater Pump.

flow. The polarization curves created based on the polarization-curve database are shown in Figure 18. The polarization curves utilized values applicable after the passage of 168 hr, when the cathodic current density was relatively stable. The conductivity of seawater was set as 4.6 S/m (20°C).

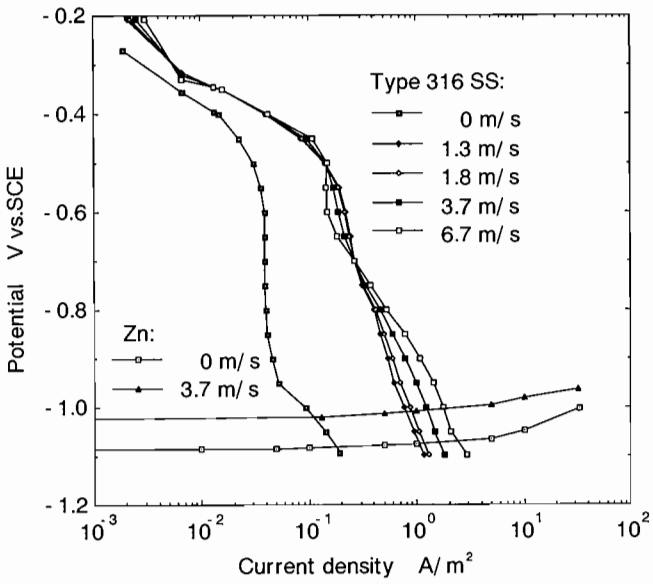

Figure 18. Polarization Curves for Boundary Element Analysis Defined by the Polarization-Curve Database.

Figure 19 is a display of the analyzed potential distribution. The entire pump surface was polarized to approximately −0.4 V versus SCE. Since the E_P of the type 316 SS is −0.32 V (Tsujikawa, et al., 1981), it was determined that all regions of the pump were protected from corrosion. On the other hand, the consumption rates of zinc anodes were calculated from the results of a current density analysis.

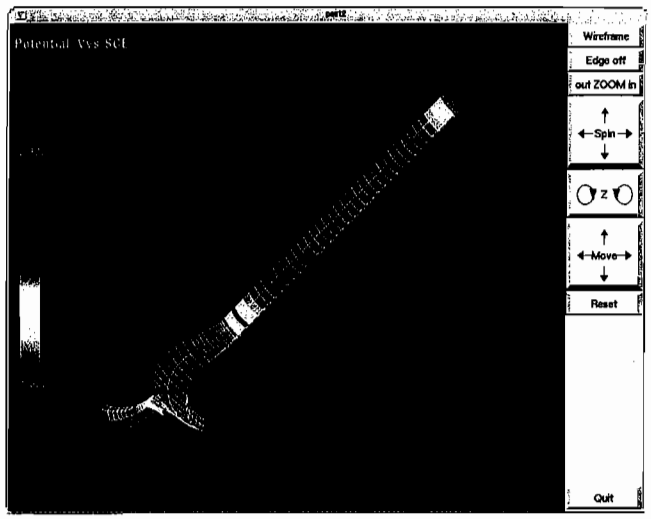

Figure 19. Display of the Potential Distribution Inside Vertical Seawater Pump.

Figure 20 shows another example of a cathodic protection analysis (potential distribution) on a double-suction volute pump made of austenitic cast-iron having a 600 mm bore diameter. This pump has a more complex structure; moreover, it is difficult to create a symmetry-based model such as that for a vertical pump. Since BEM does not require discretization of internal elements, analysis preparation and calculation convergence can be completed in a short time.

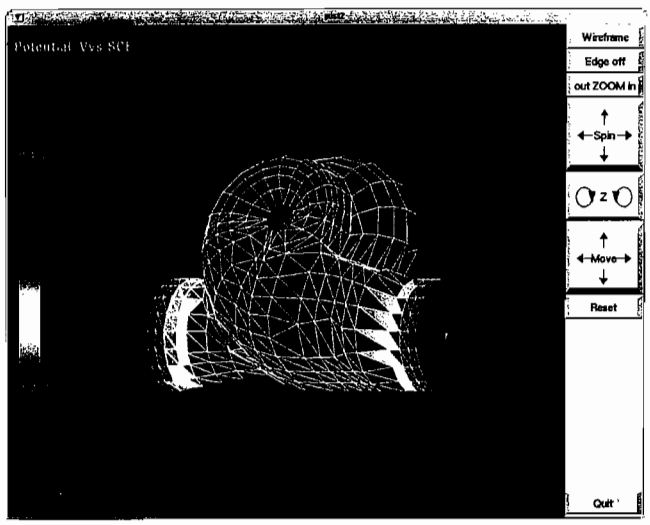

Figure 20. Cathodic Protection Analysis (Potential Distribution) On a Double-Suction Volute Pump.

CONCLUSIONS

Mechanisms and examples of galvanic corrosion and cathodic protection were explained. The authors emphasized the necessity of numerical analysis, because experiment-based methods are limited in their capacity to accurately predict galvanic corrosion

and cathodic protection involving actual equipment and structures with complex 3-D fields, and developed analysis programs based on boundary element method (BEM), which does not require discretization of internal elements.

In order to make a practical application of BEM for quantitative predictions of corrosion and corrosion protection of pumps, a BE analysis system based on the 2-D, 3-D, and axisymmetric programs were developed. The system consists of a polarization-curve database and programs to perform element discretization, input file setup, BE analysis, and graphic display of input and output data. In this system, the effect of flow-velocity and time on the polarization curve can be taken into account for defining the boundary conditions. The BE analysis system is utilized for corrosion protection design concerned with the cathodic protection and galvanic corrosion of equipment used in corrosive media, such as seawater. With this quantitative corrosion prediction technique, design, maintenance, and control operations can be streamlined, equipment reliability improved, and costs reduced through optimal designing.

Although the explanation provided in this report was abbreviated, the authors are continuing to strive to develop this technique for use in analyzing optimization problems and inverse problems of corrosion and corrosion protection (Aoki, et al., 1999).

REFERENCES

Aoki, S., Amaya, K., and Miyasaka, M., 1999, "Boundary Element Analysis of Cathodic Protection for Complicated Structures," Proc. Corrosion '99, Research Topical Symposium, Houston, Texas, NACE International, p. 45.

Aoki, S., Kishimoto, K., and Miyasaka, M., 1988, "Analysis of Potential and Current Density Distributions Using a Boundary Element Method," *Corrosion, 44*, (12), p. 926.

Aoki, S., Kishimoto, K., and Sakata, M., 1985, "Boundary Element Analysis of Galvanic Corrosion," Appl. Boundary Element VII (Eds. C.A. Brebbia and G. Maier), *1*, Springer-Verlag, pp. 1-63~1-71.

Adey, R. A. and Hang, Y., 1999, "Computer Simulation as an Aid to Corrosion Control and Reduction," Proc. Corrosion 99, Research Topical Symposium, Houston, Texas, NACE International, p. 99.

Danson, D. J. and Warne, M. A., 1983, "Current Density/Voltage Calculations Using Boundary Element Technique," Corrosion '83, Paper No. 211, Houston, Texas, NACE International.

Gartland, P. O., Bjoernaas, F., and Osvoll, H., 1999, "Computer Modeling of Offshore CP Systems for 15 Years: What Have We Learned?" Proc. Corrosion '99, Research Topical Symposium, Houston, Texas, NACE International, p. 17.

Kasper, R. G. and April, M. G., 1983, "Electrogalvanic Finite Element Analysis of Partially Protected Marine Structures," *Corrosion*, 39, p. 18.

Miyasaka, M., Amaya, K., Kishimoto, K., and Aoki, S., 1995a, "Application of BEM to Cathodic Protection of Seawater Pump," ASME PVP, *306*, p. 286.

Miyasaka, M., Kishimoto, K., and Aoki, S., 1995b, "A Study on Differential-Flow-Rate-Cell Corrosion in Seawater," Corrosion '95, Paper No. 287, Houston, Texas, NACE International.

Miyasaka, M., Kishimoto, K., and Aoki, S. 1995c, "Application of BEM to Cathodic Protection of Seawater Pump," Corrosion '95, Paper No. 288, Houston, Texas, NACE International.

Miyasaka, M., Takayama, H., Amaya, K., and Aoki, S., 1998, "Combined BEM Analysis of 3D and Axisymmetric Regions for Cathodic Protection Design of Seawater Pump," Corrosion '98, Paper No. 689, Houston, Texas, NACE International.

Strommen, R., 1979, "Current and Potential Distribution on Cathodically Protected Submarine Pipelines," Trans. Int. Mar. Wng. C. Conf., *91*, p. 74.

Tsujikawa, S., Kashiwase, M., Tamaki, K., and Hisamatsu, Y., 1981, *Boshoku-Gijyutu*, Japan Society of Corrosion Engineering, *30*, p. 62.

Zamani, N. G., Porter, J. F., and Mufti, A. A., 1986, "A Survey of Computational Efforts in the Field of Corrosion Engineering," Int. J. Numer. Methods Eng., *23*, p. 1295.